Journal Pre-proofs

Full Length Article

Nickel-Carnosine Complex: A New Carrier for Enzymes Immobilization by Affinity Adsorption

Junyang Xu, Yanjun Jiang, Liya Zhou, Li Ma, Zhihong Huang, Jiafu Shi, Jing Gao, Ying He

PII: S1004-9541(21)00206-8
DOI: https://doi.org/10.1016/j.cjche.2021.04.019
Reference: CJCHE 2241

To appear in: *Chinese Journal of Chemical Engineering*

Received Date: 31 December 2020
Revised Date: 6 April 2021
Accepted Date: 25 April 2021

Please cite this article as: J. Xu, Y. Jiang, L. Zhou, L. Ma, Z. Huang, J. Shi, J. Gao, Y. He, Nickel-Carnosine Complex: A New Carrier for Enzymes Immobilization by Affinity Adsorption, *Chinese Journal of Chemical Engineering* (2021), doi: https://doi.org/10.1016/j.cjche.2021.04.019

Article

Nickel-Carnosine Complex: A New Carrier for Enzymes Immobilization by Affinity Adsorption

Junyang Xu [1], Yanjun Jiang [1,3], Liya Zhou [1,*], Li Ma [1], Zhihong Huang [1], Jiafu Shi [2], Jing Gao [1], Ying He [1,*]

[1] School of Chemical Engineering and Technology, Hebei University of Technology, Tianjin 300130, China

[2] Tianjin Key Lab of Biomass/Wastes Utilization, School of Environmental Science & Engineering, Tianjin University, Tianjin 300072, China

[3] National-Local Joint Engineering Laboratory for Energy Conservation of Chemical Process Integration and Resources Utilization, Hebei University of Technology, Tianjin 300130, China

Corresponding Author

*E-mail: liyazhou@hebut.edu.cn(L. Zhou); heying1980@hebut.edu.cn(Y. He)

Abstract

Immobilization is an effective method to promote the application of enzyme industry for improving the stability and realizing recovery of enzyme. To some extent, the performance of immobilized enzyme depends on the choice of carrier material. Therefore, the development of new carrier materials has been one of the key issues concerned by enzyme immobilization researchers. In this work, a novel organic-inorganic hybrid material, nickel-carnosine complex (NiCar), was synthesized for the first time by solvothermal method. The obtained NiCar exhibits spherical morphology, hierarchical porosity and abundant unsaturated coordination nickel ions, which provide excellent anchoring sites for the immobilization of proteins. His-tagged organophosphate-degrading enzyme (OpdA) and ω-transaminase (ω-TA) were used as model enzymes to evaluate the performance of NiCar as a carrier. By a simple adsorption process, the enzyme molecules can be fixed on the particles of NiCar, and the stability and reusability are significantly improved. The

analysis of protein adsorption on NiCar verified that the affinity adsorption between the imidazole functional group on the protein and the unsaturated coordination nickel ion on NiCar was the main force in the immobilization process, which provided an idea way for the development of new enzyme immobilization carriers.

Keywords

Nickel carnosine complex; Organic-inorganic hybrid materials; Carrier; enzymes; Immobilization.

1. Introduction

Enzyme catalysis has been widely used in chemical industry, pharmaceutical industry, environment and many other fields thanks to its high catalytic efficiency and mild reaction conditions [1, 2]. However, the sensitivity of the enzymes to external environment and the difficulty of recycling limit their applications [3]. Enzyme immobilization is one of the effective methods to overcome these drawbacks [4-6]. Compared with free enzymes, immobilized enzymes have many advantages. For example, immobilized enzymes can reduce the dissolution of enzymes in the aqueous system, facilitate separation to achieve repeated use of catalysts and reduce the difficulty of product purification and post-processing. Under the confining of the carrier, immobilized enzymes can avoid the agglomeration of enzyme molecules and maximize the rate of enzyme catalytic reaction. Under the protection of the carrier, the reduced inactive rate of enzyme can reduce input costs and enhance the possibility of large-scale application [5-9]. In recent years, large number of literatures have reported the methods of enzyme immobilization, but the immobilized method of obtaining the biocatalysts with high activity, stability and universality is still unsatisfactory, which still limits the wide application of enzymes in industry [10]. The immobilization process will inevitably cause certain damage to the enzymes, resulting in a decrease in enzyme activity and stability [5, 6]. Therefore, the construction of new immobilization methods and carriers requires further research [7-9]. The properties of carrier materials and the interaction between carrier and enzyme molecules determine the catalytic performance of the immobilized enzymes [7, 11]. Although many kinds of materials have been reported for immobilizing enzymes, the development of controllable, multifunctional and biocompatible materials with better performance for enzymes immobilization is still required.

Organic-inorganic hybrid materials are widely investigated in the past two decades [12, 13]. They are composed of inorganic metal ions and organic ligands, which have the characteristics of ordered and adjustable porosity, variety of morphologies and high specific surface area, etc., and are

excellent carriers for biomolecule immobilization [14, 15]. Metal-organic frameworks (MOFs), as the star of hybrid materials, have been widely studied in chemical fields such as catalyst, adsorption, separation, protein loading and transport [16, 17]. For immobilizing enzymes on MOFs, the common methods include *in situ* immobilization by encapsulation or coprecipitation [18, 19], adsorption [20, 21] and covalent after surface modification [22]. The adsorption method is widely used because of its simple operation [23]. Furthermore, unlike other types of materials, the affinity adsorption between MOF materials and protein molecules also promotes its application in immobilization. For example, RÖder *et al*. [24] used the coordinative interaction of metal-organic framework with oligohistidine-tags (His-tags) to anchor different molecular units on the surface of MOFs, which is a novel concept to generate multifunctional nanosystems. The coordination unsaturated metal sites (CUS) in MOF materials can form coordination bonds with histidine imidazole groups, which is similar to the principle of immobilized metal-ion affinity chromatography. Sun *et al*. [25] fabricated a layer of Zr-group coordination polymer (Zr-cp) on hollow MnO_2 microspheres, and successfully achieved selective immobilization of His_6-DAAO by utilizing the coordination between CUS on h-MnO_2@Zr-CP and His-tag imidazole group. These reports show that MOF materials can be used as the carrier of enzyme immobilization by affinity adsorption, which provide a new approach for immobilizing enzymes.

Carnosine is one of water-soluble dipeptide, consisting of alanine and histidine that provides six potential ligand junctions: two imidazole nitrogen, one carboxyl oxygen, one amino nitrogen, and one oxygen and nitrogen of the amide bond [26]. Under different conditions, carnosine can participate in coordination with metal ions in different ligand forms [27, 28]. In this work, carnosine was used as a ligand to coordinate with nickel ions to prepare nickel-carnosine complex (NiCar) under hydrothermal conditions. NiCar was synthesized by self-templating process without template and pore-making agents, which simplifies the synthesis process, eliminates heterogeneous growth and facilitates scaling up [29]. NiCar can be used to immobilize enzymes without activation and post-

modification. OpdA and ω-transaminase (ω-TA) were used as model enzymes to evaluate the performance of NiCar as carrier. As we know, it was the first time to synthesize NiCar and used as the carrier of enzyme immobilization. The immobilization could be completed by affinity adsorption between CUS on the materials and enzymes, which provides an idea way for the design of new carriers.

2. Materials and methods

2.1. Materials

L-Carnosine (98%) was purchased from Aladdin Reagent Inc. Fluorescein isothiocyanate (FITC) was purchased from Shanghai Macklin Biochemical Co. Ltd. Nickel chloride ($NiCl_2$), N, N-dimethyformamide (DMF), and Tris(hydroxymethyl)aminomethane were purchased from Tianjin Keruisi Fine Chemical Co. Ltd. (Tianjin, China). All other reagents were purchased and used without further purification.

2.2. Characterization

SEM images and EDS of the NiCar were recorded on Nova Nano SEM450 field-emission microscope. XPS spectra were collected by a Thermo Scientific K-Alpha X-ray photoelectron spectrometer. N_2 adsorption-desorption experiment was carried out by micromeritics ASAP 2020 gas sorptometer under the condition of 77k. Fourier-transform infrared spectroscopy (FT-IR) characterization was obtained on Bruker VECTOR22 spectrometer. Fluorescent isothiocyanate (FITC) labeled enzyme was immobilized on NiCar, and then a Leica TCS SP5 microscope is used to observe the Confocal laser scanning microscopy (CLSM) micrographs.

2.3. Fabrication of NiCar

In a typical synthesis, $NiCl_2 \cdot 6H_2O$ (0.337 $mol \cdot L^{-1}$, 10 ml) and carnosine (0.45 $mol \cdot L^{-1}$, 4 ml) were dissolved in an aqueous solution respectively. A mixture of DMF (42 ml) and deionized water (4 ml) was used as the reaction medium. The ligands solution and the reaction medium were added to the reactor successively, and then the reactor was put into the oven and heated for a certain time at

180 °C. After being cooled down, the green solid was recovered by centrifugation. Finally, the powder was washed with DMF for two times and water for one time and then dry in oven at 60 °C. The products with different reaction time were characterized by SEM, and the reaction time was determined while the formation process of NiCar was analyzed.

2.4. Preparation of NiCar immobilized enzyme

To verify the role of affinity adsorption in immobilization, two recombinant enzymes, His-tagged OpdA and ω-TA, were used to verify performance of NiCar as carrier. In order to analyze the interaction between enzyme and carrier, the cell lysate of expressing enzyme was selected as the initial enzyme solution. The crude enzyme solution, the adsorbed supernatant and the desorbed protein were analyzed by sodium dodecyl sulfate polyacrylamide gel electrophoresis (SDS-PAGE). The expression of enzymes was prepared based on our previous work [30-32]. The gene sequences of OpdA and ω-TA were from *Agrobacterium radiobacter* P230 and *Chromobacterium violaceum*, respectively. After codon optimization, they were expressed in *E. coli* with pET-28a as vector.

NiCar was mixed with 1 mL enzyme and shaking at ambient temperature to realize the immobilization of enzyme. Enzyme-bound NiCar was isolated and washed several times with Tris-HCl buffer with low concentration imidazole (40 mmol·L^{-1}) to remove the unabsorbed proteins after incubation for some time. The obtained biocomposites were denoted as enzyme@NiCar. The immobilization process was optimized by adjusting the adsorption time and the mass ratio of NiCar to enzyme. The mass ratio between NiCar and enzyme was fixed at 5:1. After incubation for different time, the protein loading on the carriers was determined by Bradford assay method. Different mass of carriers was mixed with 1 ml enzyme solution (the mass ratio of the carriers to the protein was set from 2:1 to 10:1). After incubation for the same time, the protein loading and specific activity of the enzyme@NiCar was determined. The measurement of enzyme activity was based on our previous studies [30, 31]. The activity recovery and immobilization efficiency of enzyme@NiCar were calculated by the following equations:

$$\text{Activity recovery} = \frac{\text{Activity of enzyme@NiCar (U)}}{\text{Initial activity of enzyme in cell lysates (U)}} \times 100\% \quad (1)$$

$$\text{Immobilization efficiency} = \frac{\text{Immobilized protein (mg)}}{\text{Total proteins in cell lysates (mg)}} \times 100\% \quad (2)$$

2.5. Enzymatic properties of free enzymes and enzyme@NiCar

To investigate the optimum reaction conditions, the enzymatic activity of free OpdA and OpdA@NiCar was determined under different temperature (30-60^{o}C) in Tris solution (50 mmol·L^{-1}, pH 8). The data of enzyme activity were converted into relative activity for analyzing the change trend of free enzyme and immobilized enzyme at different temperatures. Similarly, free OpdA and OpdA@NiCar were dispersed in buffers with different pH (5-12) to analyze the effect of pH on enzyme activity. Kinetic parameters of enzymes were obtained by the following methods. In the reaction of OpdA degradation methyl parathion, the reaction rates at different substrate concentrations were measured, and then the Michaelis-Menten parameters were obtained by nonlinear fitting in the growth model.

The stability of free OpdA and OpdA@NiCar was studied by the following methods. Free enzyme and immobilized enzyme were incubated at 50 and 60^{o}C respectively to study the thermal stability. After incubation at different times (take samples every 1 hour), the samples were transferred to ice water for 5 min, then the residual activity was measured. The change of enzyme activity with incubation time was analyzed by using the enzyme activity before incubation as the benchmark. Free OpdA and OpdA@NiCar were dispersed in buffers with extreme pH 4 and 12, respectively. After incubation at different times (take samples every 1 hour), the residual activity was determined for analyzing the pH stability.

The reusability of the OpdA@NiCar was determined by degradation of methyl parathion. OpdA@NiCar was dispersed in the reaction system and then separated by centrifugation after 10 minutes. The concentration of 4-nitrophenol in supernatant was determined to calculate the enzyme activity. The isolated OpdA@NiCar was washed three times with a fresh buffer and then redispersed

in the new reaction system for the next batch of reactions. This process was repeated ten times, and the relative value of enzyme activity was transformed to analyze the reusability of the OpdA@NiCar. OpdA@NiCar and free OpdA were stored in the refrigerator (4^{o}C), and the residual activity after different storage time was measured to investigate the storage stability.

The method for determining the enzymatic properties of ω-TA and ω-TA @NiCar was basically consistent with the above method.

3. Results and Discussion

3.1. Fabrication and characterization of NiCar

The spherical NiCar with hierarchically porous structure was synthesized by the coordination and crystal transformation of nickel ion and carnosine in the mixed solvent of DMF and water (total volume ratio: 7:3) by hydrothermal method. In the synthesis process, template and pore-making agents were not needed.

3.1.1. The formation of NiCar

The products obtained from heating at 180 ^{o}C at different times were denoted as NiCar (X) (X stands for heating time, X=1, 3, 5h). The SEM images of NiCar (X) were shown in Figure 1a-c. NiCar (1h) exhibited a spherical shape, with smooth, flat and dense surface and no obvious pore structure (Figure 1a). With the extension of heating time, the surface of NiCar (3h) became rough and pores appeared on the particle surface (Figure 1b). Further extending the heating time, the surface of NiCar (5h) became rougher and mesopore or even macropore apparently appeared (Fig. 1c). According to the SEM results, NiCar first produced the solid sphere structure with smooth surface by the coordination of nickel ion and carnosine. With the increase of heating time, the structure of NiCar started to transform from the surface to the inside of the particles with itself as the template. In this transformation process, the solid structure of NiCar was destroyed, and the pore structure began to appear on the particles. With the increase of heating time, the pore changed from micropore to mesopore or even macropore.

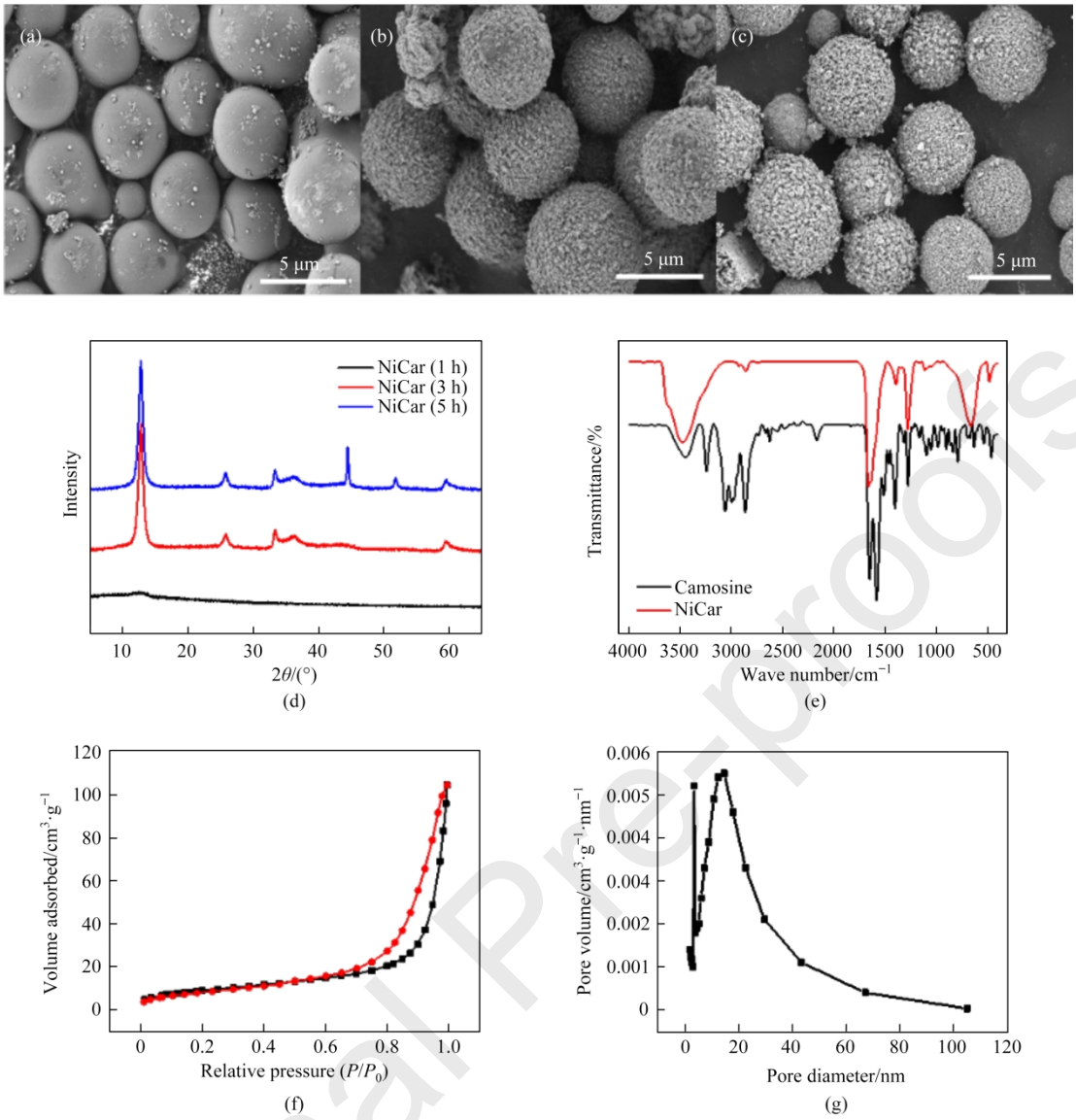

Figure 1 SEM images of (a) NiCar (1h), (b) NiCar (3h) and (c) NiCar (5h); (d) Powder XRD patterns of NiCar; (e) FT-IR spectra of carnosine and NiCar; (f) N_2 adsorption-desorption isotherms and (g) pore size distribution profile of NiCar.

Furthermore, we characterized the samples at different heating times with XRD, and the results were shown in Figure 1d. There was no obvious diffraction peak in the XRD pattern of NiCar (1h), and it was only slightly prominent around 12 ° in 2θ, indicating NiCar (1h) was amorphous. However, NiCar (3h) had obvious diffraction peaks at 12°, 26°, 33°, 36° and 59 °, which may be diffraction peaks of a crystalline substance formed by coordination of nickel ions and carnosine molecules. With the increase of heating time, the XRD pattern of NiCar (5h) showed new changes on the basis of

NiCar (3h), and new diffraction peaks appeared around 44.5°, 52° and 76 °, which were consistent with the diffraction peaks of nickel [33]. This indicated that with the accumulation of energy, the morphology of NiCar was further transformed. In addition to coordination, the redox reaction between nickel ions and carnosine might occurred, leading to the appearance of nickel. As shown in the XRD results, with the increase of heating time, NiCar gradually transformed from amorphous state to crystalline, which also confirms the change of morphology in the formation of NiCar proposed above. Considering that NiCar was used for affinity adsorption of enzyme immobilization, mesoporous structure was an important property for the carrier [11, 34]. In combination with the reaction operation, we selected NiCar (3h) as the follow-up research material. In the following research, the carrier was denoted as NiCar.

To verify the coordination relationship between nickel ion and carnosine, the chemical composition and structure of NiCar were analyzed by comparing the FT-IR spectra of carnosine and NiCar (Figure 1e). Peaks at 1512 and 3062 cm^{-1} were assigned as the N-H vibration peaks of amide-II and imidazole rings in carnosine, and peak at 1583 cm^{-1} was assigned as the carboxyl stretching vibrations of carnosine [35]. However, these peaks became weak or disappeared in the spectrum of NiCar, suggesting a possible coordination between carnosine and nickel ions. There were many coordination forms between carnosine and metal ions [26]. As a multidentate ligand, carnosine can provide six potential coordination sites: two imidazole nitrogen (N^1 and N^3), one carboxylate oxygen (O), one amino nitrogen (N), and one oxygen and nitrogen of the amide bond (O and N). In the complex of copper and carnosine (Cu/Car), the coordination sphere around the Cu^{2+} center was conformed by the terminal amino nitrogen, the amide nitrogen, a carboxylate oxygen of carnosine molecules, and the N^3 nitrogen of the imidazole moiety of the second peptide molecule of the dimer [36]. The complex composition of carnosine and zinc is similar to that of copper, but existed in the form of polymers. Another coordination form existed between zinc and carnosine. In ZnCar (an MOF synthesized with zinc ions and carnosine), Zn^{2+} bind to the amino N, carboxyl O and two N atoms of

the imidazole group of carnosine in the form of 4 coordination [28]. By comparing the XRD and FT-IR results, the coordination between Ni^{2+} and carnosine in NiCar was similar to that of Cu/Car, in which Ni^{2+} were connected to the terminal amino N, the N and O in the peptide bond and the N^3 in the imidazole group.

3.1.2. The morphology and pore structure of NiCar

As shown in Figure 1b, the obtained NiCar (the heating time was 3h) presented a rough spherical surface morphology with a particle size of about 5μm. The spherical structure of NiCar was formed by the accumulation of small particles, and the surface of the complex has obvious pore structure. The rough surface and large pore structure of NiCar particles facilitate the adsorption of enzyme molecules on the material during immobilization [11]. The pore structure of NiCar particles was analyzed by N_2 adsorption-desorption isotherms. As shown in Figure 1f, the isotherms were identified as type IV, which indicated the hierarchically mesoporous and microporous structures [37]. The obvious H1 type hysteresis loops appeared on the desorption curve of NiCar, which was a sign of the existence of mesoporous structure directly connected with the particle surface [38, 39]. The pore size distribution of NiCar was analyzed by BJH pore-size mode. Two peaks appeared in the pore diameter distribution curve of NiCar (Figure 1g), which were 2 nm and 20 nm respectively. It was speculated that the pore diameter of 2 nm was the pores on the small particles of the complex, while 20 nm might be the pores generated by the stacking of small particles or layers, which were consistent with the results observed by SEM.

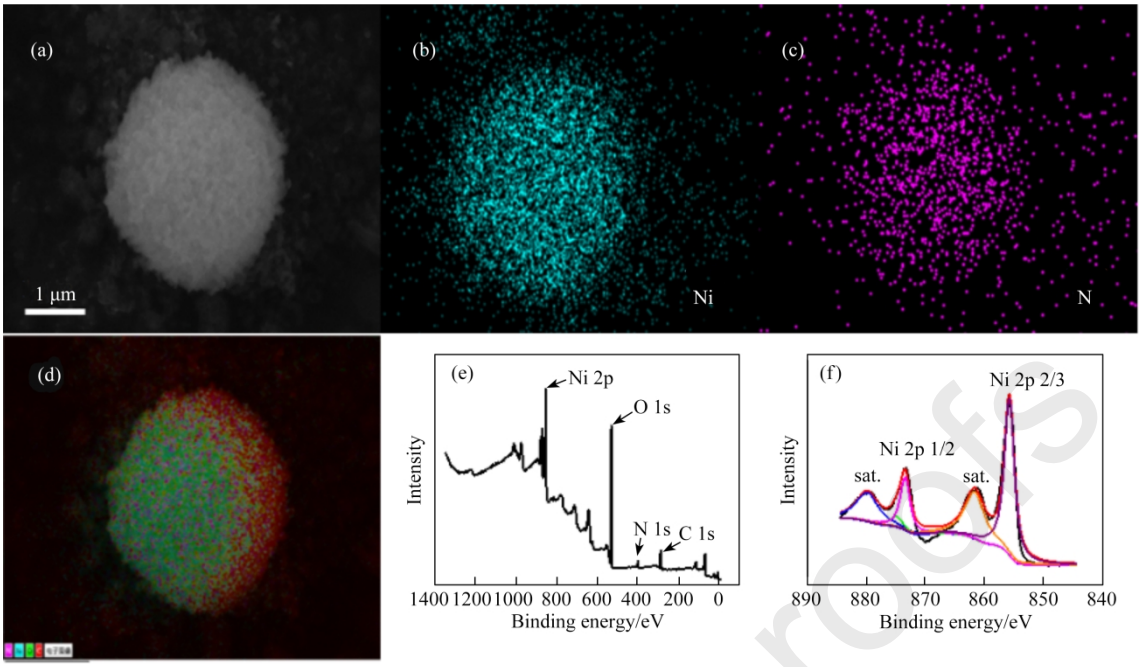

Figure 2 (a) SEM image and elemental mappings of NiCar: (b) Ni element, (c) N element and (d) overlay image; XPS spectra of NiCar: (e) survey scan and (f) Ni 2p.

3.1.3. Distribution and chemical state of nickel ions in NiCar

For affinity adsorption, the main force is the interaction between the unsaturated coordination metal ions in the materials and the imidazole functional group of histidine in the protein. Therefore, the state and distribution of metal ions in the carrier materials have important effects on the immobilized enzyme by affinity adsorption. Based on this, the distribution and chemical valence states of nickel ions in NiCar were analyzed. EDS mapping was used to study the elements distribution of NiCar nanoparticles. As shown in Figure 2a-d, C, N, O and Ni can be observed, in which C, N and O came from carnosine and nickel ion from nickel chloride. This also indicated that carnosine and nickel ion exist in NiCar at the same time. Nickel elements distributed uniformly throughout the spherical particles of NiCar. The valence states of nickel ions on NiCar surface were examined with XPS. Four characteristic peaks for C 1s, N 1s, O 1s, and Ni 2p were clearly observed in the scan of NiCar (Figure 2e), which agreed with the EDS analysis. The 2p 3/2 and 2p 1/2 peaks of Ni 2p, located at 855.4 eV and 873.3 eV respectively, was shown in Figure 2f, which indicated that bivalence was the main form of Ni in NiCar [40, 41]. The appeared at 861.2 eV and 879.9 eV

were the satellite peaks of nickel ions [42]. The uniform distribution of unsaturated coordination nickel ions in NiCar provides a potential coordination site for protein adsorption, which indicated that NiCar has the potential as an affinity adsorption carrier for immobilized enzymes.

3.2. NiCar immobilized enzymes by affinity adsorption

3.2.1. Immobilization of OpdA on NiCar

OpdA is an enzyme that can catalyze the degradation of organophosphorus pesticides, which can degrade methyl parathion into *p*-nitrophenol [43, 44]. In this work, OpdA was selected as the model enzyme to verify performance of NiCar as carrier. OpdA was expressed in *E. coli.* by recombinant plasmid pET-28a (+)-OpdA. The supernatant of cell lysates after ultrasonic crushing and centrifugation was used as the crude enzyme solution for subsequent experiments. Here, unpurified cell lysate expressing the enzyme was used as the initial enzyme solution to verify the effect of affinity adsorption. To realize the immobilization, a certain amount of NiCar was incubated with the cell lysates containing His-tagged OpdA under shaking condition. After 3 hours of incubation, enzyme-bound NiCar was isolated and washed several times with low concentration imidazole buffer (40 $mmol \cdot L^{-1}$) to remove the unabsorbed proteins, and the obtained biocomposites were denoted as OpdA@NiCar.

To select the best immobilization parameters, the time required to reach adsorption equilibrium was firstly studied with 5:1 mass ratio of NiCar to total protein. As can be seen from the graph of the protein loading (Figure 3c), after 2h of incubation, there was no obvious change, indicating that the adsorption balance between NiCar and the protein was reached. The amount of support affects the characteristics of the immobilized enzyme, so the dosage of NiCar was also investigated. The support and protein with different mass ratios were incubated under the same conditions for 2 hours. The amount of support was determined by comparing the protein loading with the activity of the biological complex. When the mass ratio of NiCar to the enzymes was 4:1, the maximum protein loading was 59.69 mg/g support (Figure 3d) and the immobilization efficiency was 23.87%. As the amount of

NiCar increased further, the protein loading began to decline, which may be caused by the excess of NiCar. The specific activity of OpdA@NiCar showed a decreasing trend, possibly because the enzyme active site was obscured by the excessive adsorption of protein [45]. The mass transfer resistance caused by the multi-layer adsorption was also a possible reason for the decrease of enzyme activity. Finally, the ratio of NiCar to total protein of 4:1 was selected as the dosage of NiCar. Under this condition, the specific activity of OpdA@NiCar was 745.76 U/g protein， and the enzyme activity recovery was 77.18%. Fluorescence labeling can be visually demonstrated the adsorption and distribution of the protein on NiCar, so fluorescein isothiocyanate (FITC) labeled cell lysates containing OpdA was prepared and used for immobilization in the same conditions. Green fluorescent signal shown in Figure 3a proved that the FITC-labeled enzyme was successfully adsorbed and distributed on NiCar.

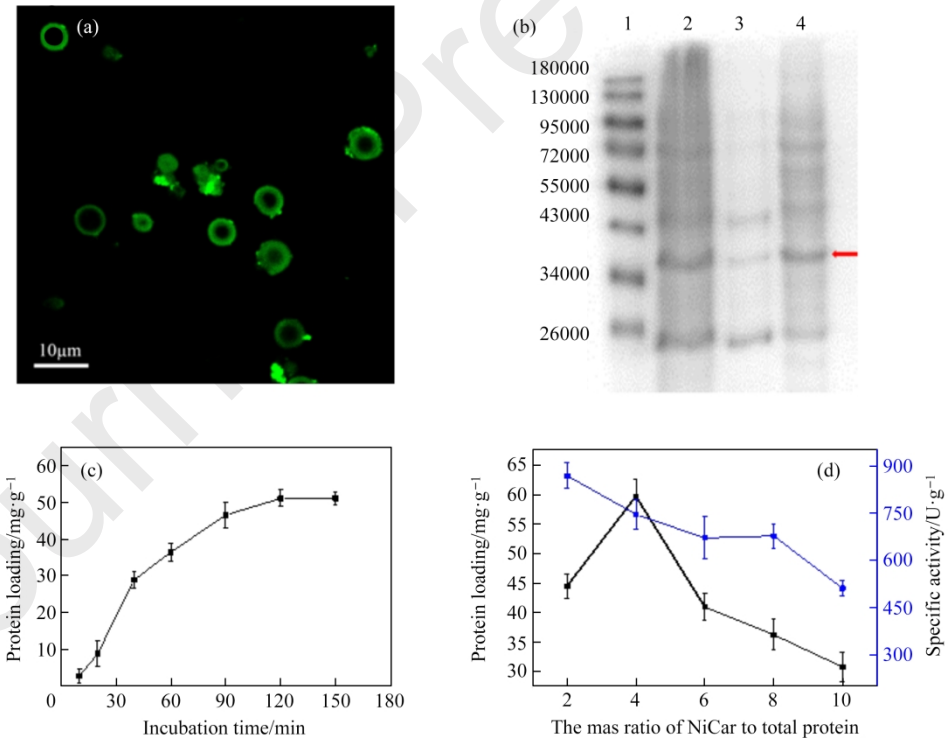

Figure 3 (a) Confocal laser scanning microscopy image of OpdA@NiCar; (b) SDS-PAGE analysis of OpdA (Lane 1, marker; lane 2, cell lysates; lane 3, supernatant after immobilization by NiCar; lane 4, eluted protein from NiCar); (c) Adsorption equilibrium curve of NiCar to total protein at 5:1 ratio (w/w); (d) Protein loading and activity of immobilized OpdA at different ratios (w/w) of

NiCar to total protein.

The electrostatic interaction, hydrogen bond and intermolecular interaction were the main interactions in enzyme immobilization by physical adsorption. Compared with these forces, the affinity adsorption between metal ions and proteins has a stronger interaction. To analyze the interaction between NiCar and OpdA, we compared the initial protein solution, the adsorbed supernatant and the eluted protein solution from the carrier by SDS-PAGE (Figure 3b). The target protein, OpdA, was recombined with a histidine tag, which increased the content of histidine in the enzyme and thus enhanced the carrier affinity adsorption of the target protein with unsaturated coordination nickel ions. Compared with the protein solution before immobilization (lane 1), the corresponding protein bands can be observed in the lanes of the protein eluted from the carrier (lane 3), indicating that the protein can be successfully absorbed by NiCar. The protein bands in lane 3 were further analyzed. The staining depth indicated the difference in the amount of proteins adsorbed on the carrier. A contrasting strip appears at 38,000 on lane 3, which was consistent with the mass of His-tagged OpdA [46], indicating that OpdA as the target protein was the main adsorbed protein on the carrier. Compared with other proteins, the significant adsorption of target enzyme was mainly caused by the affinity interaction between the histidine tag on OpdA and the unsaturated coordination nickel ion on NiCar. This is consistent with our expectation that affinity adsorption plays a primary role in the process of immobilization.

3.2.2. The enzymatic properties, stability and reusability of OpdA@NiCar

It can be found that the optimal reaction conditions of OpdA@NiCar were different from free OpdA by measuring the activity of free OpdA and OpdA@NiCar at different temperatures and pH. Temperature has great influence on free OpdA. Within the optimal temperature range, the enzyme activity was high. When the temperature was lower or higher than the optimal temperature, the enzyme activity was lost to different degrees. As shown in Figure 4a, optimum reaction temperatures for free OpdA and OpdA@NiCar were 45 ^{o}C and 50 ^{o}C, respectively. Compared with free enzymes,

the immobilized enzymes may require more activation energy, which resulted in an increased optimal temperature of OpdA@NiCar [47]. Similarly, the optimal pH of OpdA@NiCar also changed. The activity changes of free OpdA and OpdA@NiCar in buffers with different pH values were presented in Figure 4b. Under alkaline conditions, the activities of free enzymes and immobilized enzymes were basically unchanged, which may be attributed to that OpdA was an alkaline enzyme and more stable under alkaline conditions [48]. After immobilization, the optimal pH of immobilized OpdA moved from 9 to 8. This may be due to more hydroxide ions were adsorbed around NiCar, which caused the microenvironment of OpdA@NiCar to be alkaline and the optimum pH changed [49].

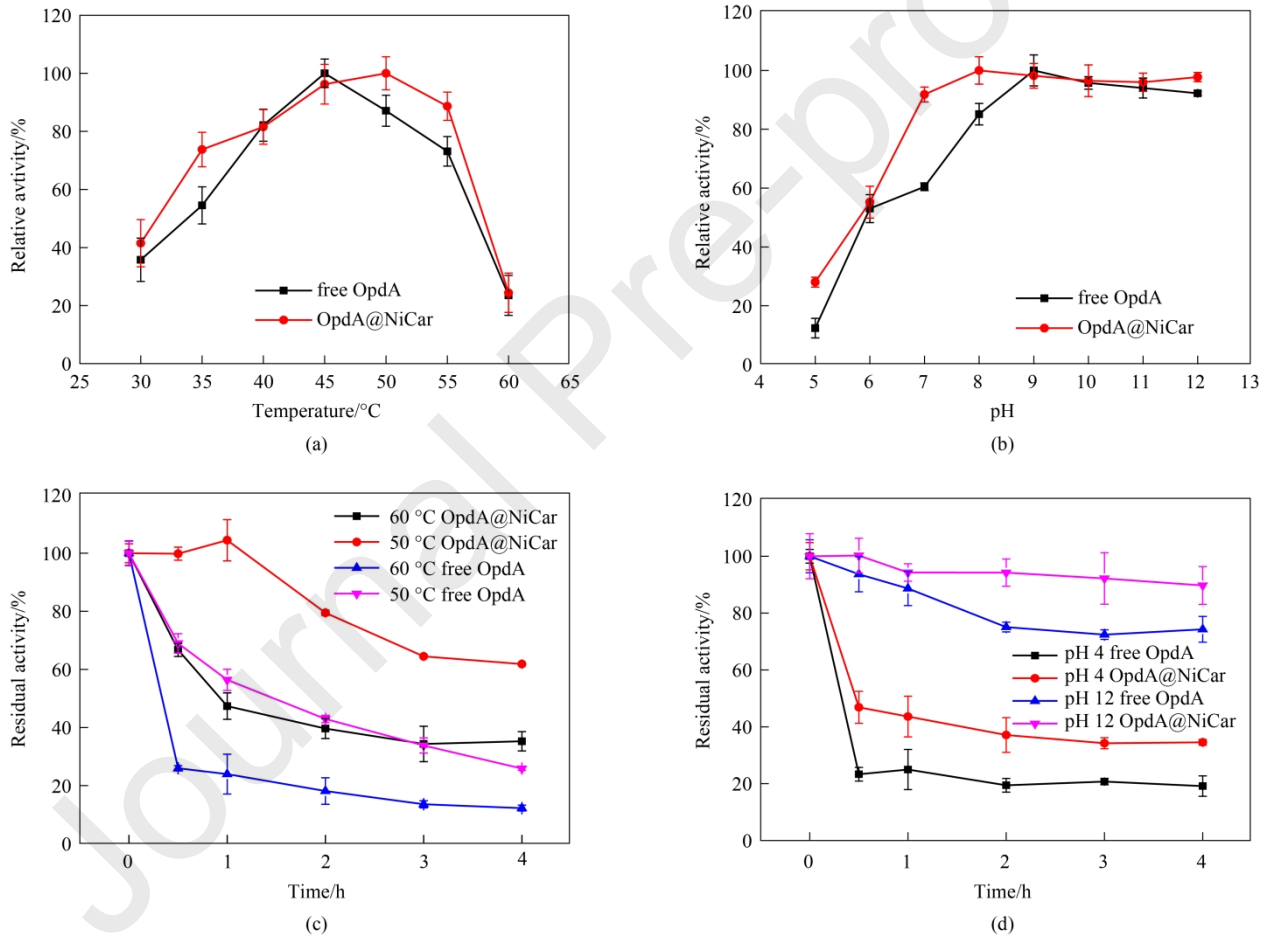

Figure 4 (a) Optimum temperature of free OpdA and OpdA@NiCar; (b) Optimum pH of free OpdA and OpdA@NiCar; (c)Thermal and (d) pH stabilities of free OpdA and OpdA@NiCar.

The kinetics of free OpdA and OpdA@NiCar were determined to further investigate the effect of immobilization on OpdA (Table 1). Compared with free OpdA, the Km value of OpdA@NiCar

increased slightly, which was 232.92 μmol· L^{-1} and 177.34 μmol· L^{-1}, respectively. The maximum reaction rate decreased from 25.51μmol·L^{-1}·min^{-1} to 19.99 μmol·L^{-1}·min^{-1} after immobilization. The changes of kinetic parameters may be due to the shielding of the active sites of the enzyme molecules during the immobilization process and the spatial conformational changes, thus resulting in the increase of the contact barriers between the enzyme molecules and the substrate [50, 51].

Table 1 The kinetic parameters for free OpdA and OpdA@NiCar

Kinetic parameters	Methyl parathion	
	Free OpdA	OpdA@NiCar
K_m /μmol·L^{-1}	177.34	232.92
V_{max} /μmol·L^{-1}·min^{-1}	25.51	19.99

We incubated free OpdA and OpdA@NiCar at high temperature (50 and 60 °C) and extreme pH (4 and 12) to study the stability of enzyme. The results of thermal stability were shown in Figure 4c, and OpdA@NiCar exhibited good performance. With the increase of treatment time at high temperature, the enzyme activity decreased to different degrees. After immersion at 50 °C for 4 hours, the free OpdA only remained 35% of the activity, while OpdA@NiCar remained 62%. After incubation 60 °C, the activity of both free enzyme and immobilized enzyme was greatly lost, and the activity of free enzyme decreased rapidly while the immobilized enzyme decreased relatively slowly. Although the loss of enzyme activity was serious, the immobilized enzyme still had obvious advantages over the free enzyme after four hours of treatment. The pH stability of OpdA@NiCar was also improved (Figure 4d). This may be due to the protective effect of NiCar on the enzyme, which made OpdA in a more suitable microenvironment and improved its stability. As can be seen from Figure 6c and d, under extreme conditions (60 °C and pH 4), the protective effect of the carrier on the enzyme was reduced. Since the enzyme was mainly distributed in the surface layer of the carrier, its activity was still affected by the environment. However, compared with the free OpdA, the OpdA@NiCar was still with obvious advantages.

After immobilization, OpdA@NiCar can be collected from the solution by centrifugation and used for the next batch of reactions after cleaning, to realize the recycling of enzyme. It was verified by reusability experiment, the residual activity of OpdA@NiCar still retains 74% after 10 cycles in methyl parathion degradation (Figure 5). Decreased activity of OpdA@NiCar was mainly due to the leakage and deactivation of OpdA@NiCar in the process of washing and recycling [52]. After 20 days of storage, OpdA@NiCar still retained 89.26% of the initial activity, while the activity of free enzyme was only 50.37% of the initial activity, which demonstrated the protective effect of NiCar on OpdA. Compared to our previous work [30, 53]， OpdA@NiCar showed improved thermal, reusability and storage stability.

To further understand the performance of NiCar, the Ni Affinity Chromatography Media (Ni-ACM), a commercial Ni-IDA modified agarose microsphere, was used as a contrast material. For OpdA, the protein loading of Ni-ACM was 31.52mg/g support, and the specific activity of OpdA@Ni-ACM was 832.44 U/g protein. The immobilization efficiency and enzyme activity recovery were 12.61% and 86.15%, respectively. Compared with NiCar, Ni-ACM had a lower protein loading but a higher enzyme activity recovery, which may be due to the strong specific binding ability of Ni-ACM to histidine tags. However, the protective effect of Ni-ACM on OpdA was relatively weak. In the investigation of reusability, the residual activity of OpdA@Ni-ACM was much lower than that of OpdA@NiCar after 10 times repeated (21.27% *v.s.*74.34%). In the test of storage stability, OpdA@NiCar also showed higher stability, which may be related to the particle and pore size of the carrier material. The enzyme molecules could only attach on the surface of Ni-ACM, where the protective effect was relatively smaller.

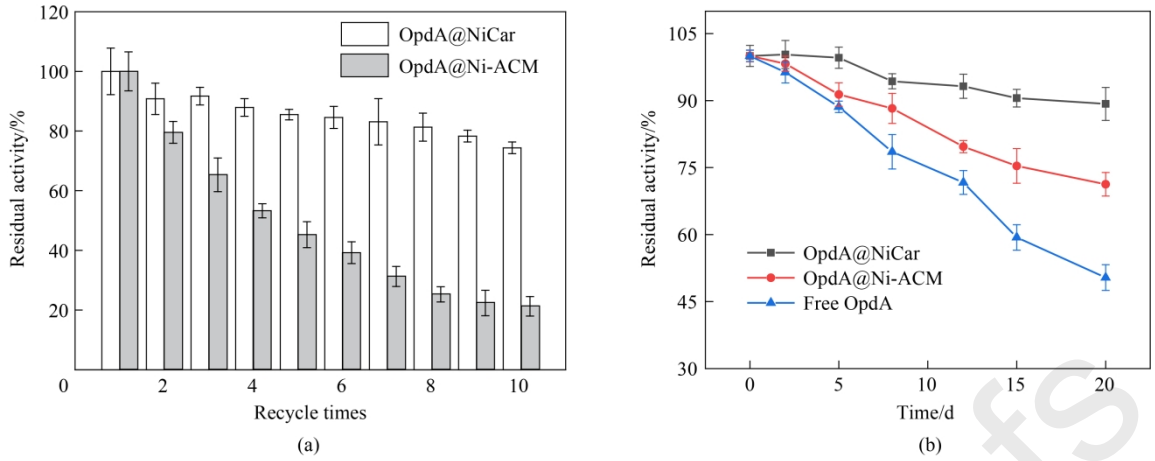

Figure 5 (a) Reusability and (b) storage stability of free and immobilized OpdA.

3.2.3. Universality of NiCar for immobilizing enzyme using affinity adsorption

As another model enzyme, ω-transaminase (ω-TA) was used to demonstrate the universality of NiCar in the affinity adsorption of His-tagged proteins. The His-tagged ω-TA was obtained by heterologous expression in *E. coli.* [31]. The same method was used for the immobilization of ω-TA on NiCar. A certain amount of NiCar was co-incubated with cell lysates to realize the immobilization of His-tagged ω-TA, which was named as ω-TA@NiCar. After optimizing the immobilization conditions, it was found that the adsorption balance between protein and NiCar was basically reached when the adsorption time was 2 hours (Figure 6c). When the mass ratio between NiCar and the protein was 4:1, the specific activity of ω-TA@NiCar was the highest, and the specific activity and protein loading, was 363.01 U/g protein and 42.92 mg/g support, respectively (Figure 6d). The enzyme activity recovery and immobilization efficiency were 53.28% and 17.17%, respectively. Compared with the preparation process of OpdA@NiCar and ω-TA@NiCar, the adsorption time of the carrier to the protein reached the equilibrium was also about 2 hours. When the activity of the enzyme@NiCar was the highest, the mass ratio between the carrier and the protein was also 4:1, which indicated that the adsorption process of NiCar to different enzymes was similar.

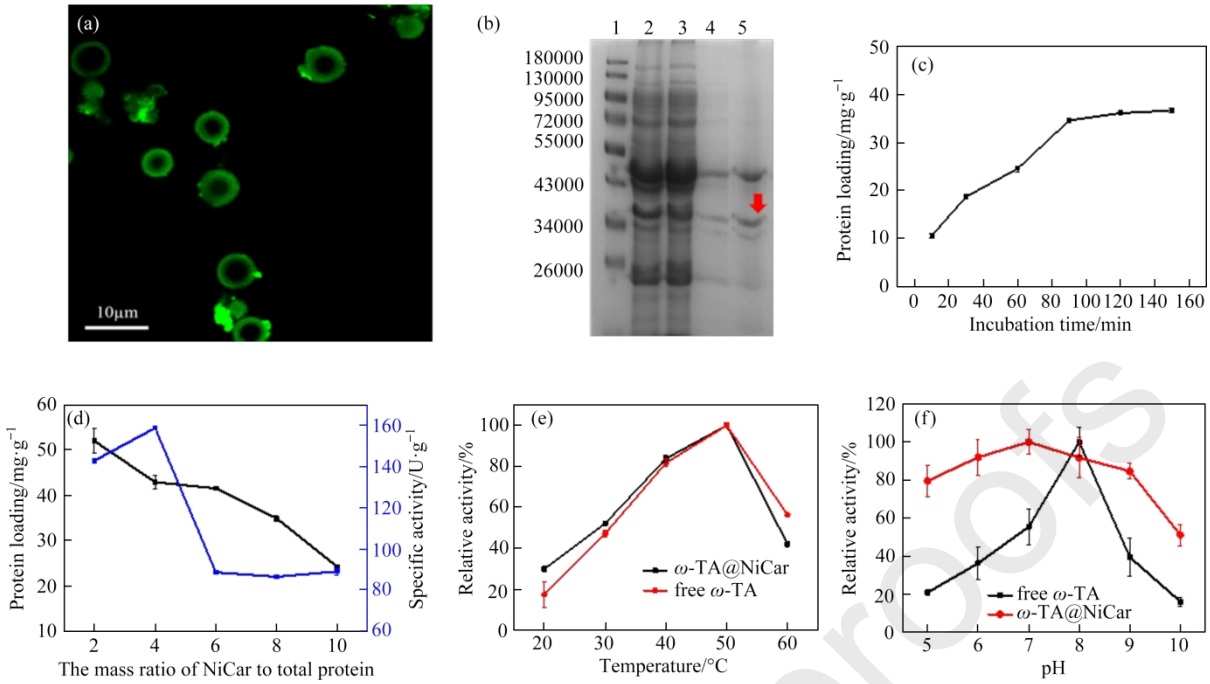

Figure 6 (a) Confocal laser scanning microscopy image of ω-TA@NiCar; (b) SDS-PAGE analysis (Line 1-maker; Line 2-cell lysate; Line 3-supernatant; Line 4-clean supernatant; Line 5-eluted protein); (c) Protein loading of His-tagged ω-TA with different adsorption time; (d) Protein loading and activity of immobilized ω-TA at different weight of NiCar; Effect of (c) reaction temperature and (d) pH on the activity of free ω-TA and ω-TA@NiCar.

The immobilization of ω-TA on NiCar was also characterized and analyzed. The green fluorescence in confocal laser scanning microscopy image (Figure 6a) proved the successful immobilization of ω-TA on NiCar. Similar to OpdA, green fluorescence representing the ω-TA appeared on the periphery of NiCar, indicating that the enzyme was adsorbed on the carrier particle. To verify the adsorption of proteins, the cell lysates, supernatant, eluent of low-concentration imidazole buffer and eluent of high-concentration imidazole buffer were also analyzed by SDS-PAGE. It was can be seen in Figure 6b, a clear target band (indicated by the red arrow) in lane 5 can be seen in the electrophoretogram, indicating that ω-TA had been immobilized successfully. It can be seen from the comparison of the protein bands (lane 5) that the target protein with the histidine tags still adsorbed more on NiCar, which indicated that affinity adsorption played a major role in the immobilization of ω-TA.

The thermal (Figure 6e) and pH (Figure 6f) stabilities of ω-TA were also improved after immobilization. Although the protein was adsorbed on the surface of the carrier and the carrier had less protective effect on the protein, the performance of the ω-TA@NiCar was still better than the free ω-TA. After immobilization, the change trend of the kinetics constant of ω-TA@NiCar was consistent with that of OpdA@NiCar (Table 2), which indicated that enrichment and immobilization of the enzyme by the present method might cover up the active sites or change the conformation of enzymes [50], resulting in decreased affinity between the enzyme and the substrate.

Table 2 Kinetic parameters of ω-TA and ω-TA@NiCar

Kinetic parameters	(*S*)-α-phenylethylamine affinity	
	Free ω-TA	Immobilized ω-TA
K_m/mmol·L^{-1}	92.42	128.81
V_{max} /mmol·L^{-1}·min^{-1}	22.71	15.76

Ni-ACM was also used as contrast material to evaluate the adsorption and immobilization capacity of NiCar on ω-TA. Under the same conditions, the protein loading of Ni-ACM was 29.31 mg/g support, and the specific activity was 412.95 U/g protein. The immobilization efficiency and enzyme activity recovery were 11.72% and 65.23%, respectively. Compared with ω-TA@Ni-ACM, ω-TA@NiCar showed higher protein loading and stability (Figure 7). After 8 times reuse, ω-TA@NiCar retained 35.03% of its initial activity, while ω-TA@Ni-ACM retained only 17.55%. After 20 days of storage, ω-TA@NiCar and ω-TA@Ni-ACM could retain 62.75% and 55.83% of their initial activity, respectively. These results indicated that NiCar can be used as a novel carrier for enzyme immobilization by affinity adsorption.

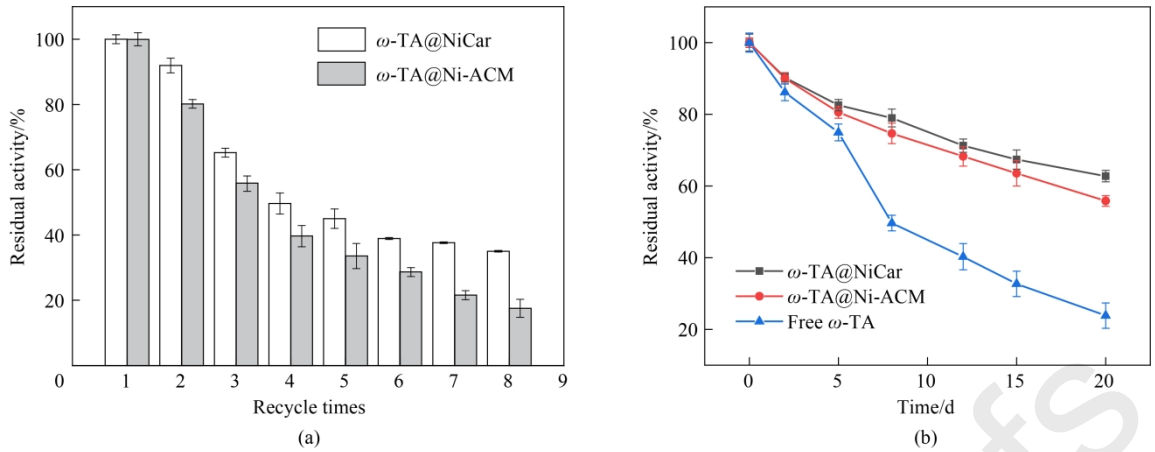

Figure 7 (a) Reusability and (b) storage stability of free and immobilized ω-TA.

4. Conclusions

In summary, a novel hybrid material, nickel-carnosine complex (NiCar), was synthesized by a simple method. The resultant NiCar exhibited spherical morphology, hierarchical porosity and abundant nickel ions, which provided the possibility to serve as a carrier for affinity adsorption of enzymes. The performance of NiCar as a carrier was evaluated by using His-tagged OpdA and ω-TA as model enzymes. After immobilization, the stability of the two model enzymes was obviously improved. By analyzing the adsorption of proteins on carrier particles, affinity adsorption was the main force for immobilizing enzyme on NiCar, which verified that the coordination of unsaturated metal ions and imidazole functional groups could be a potential way to design and develop the new carriers for enzyme immobilization.

References

[1] S. Jemli, D. Ayadi-Zouari, H.B. Hlima, S. Bejar, Biocatalysts: application and engineering for industrial purposes, *Crit. Rev. Biotechnol.*, 36 (2016) 246-258.

[2] R.A. Sheldon, J.M. Woodley, Role of biocatalysis in sustainable chemistry, *Chem. Rev.*, 118 (2017) 801-838.

[3] R.A. Sheldon, S.V. Pelt, Enzyme immobilisation in biocatalysis: why, what and how, *Chem. Soc. Rev.*, 42 (2013) 6223-6235.

[4] R.C. Rodrigues, C. Ortiz, á. Berenguer-Murcia, R. Torres, R. Fernández-Lafuente, Modifying

enzyme activity and selectivity by immobilization, *Chem. Soc. Rev.*, 42 (2013) 6290-6307.

[5] X. Wu, M. Hou, J. Ge, Metal–organic frameworks and inorganic nanoflowers: a type of emerging inorganic crystal nanocarrier for enzyme immobilization, *Catalysis Science & Technology*, 5 (2015) 5077-5085.

[6] J. Cui, S. Jia, Optimization protocols and improved strategies of cross-linked enzyme aggregates technology: current development and future challenges, *Crit. Rev. Biotechnol.*, 35 (2015) 15-28.

[7] M. Bilal, T. Rasheed, Y. Zhao, H.M.N. Iqbal, J. Cui, "Smart" chemistry and its application in peroxidase immobilization using different support materials, *Int. J. Biol. Macromol.*, 119 (2018) 278-290.

[8] J. Cui, S. Ren, B. Sun, S. Jia, Optimization protocols and improved strategies for metal-organic frameworks for immobilizing enzymes: Current development and future challenges, *Coord. Chem. Rev.*, 370 (2018) 22-41.

[9] S. Ren, C. Li, X. Jiao, S. Jia, Y. Jiang, M. Bilal, J. Cui, Recent progress in multienzymes co-immobilization and multienzyme system applications, *Chem. Eng. J.*, 373 (2019) 1254-1278.

[10] A. Liese, L. Hilterhaus, Evaluation of immobilized enzymes for industrial applications, *Cheminform*, 42 (2013) 6236-6249.

[11] D.I. Fried, F.J. Brieler, M. Fröba, Designing inorganic porous materials for enzyme adsorption and applications in biocatalysis, *Chemcatchem*, 5 (2013) 862-884.

[12] J.S. Qin, S. Yuan, C. Lollar, J. Pang, A. Alsalme, H.C. Zhou, Stable metal-organic frameworks as a host platform for catalysis and biomimetics, *Chem. Commun.*, 54 (2018) 4231-4249.

[13] J. He, S. Sun, M. Lu, Q. Yuan, Y. Liu, H. Liang, Metal-nucleobase hybrid nanoparticles for enhancing the activity and stability of metal-activated enzymes, *Chem. Commun.*, 55 (2019) 6293-6296.

[14] C. Doonan, R. Ricco, K. Liang, D. Bradshaw, P. Falcaro, Metal-organic frameworks at the biointerface: synthetic strategies and applications, *Acc. Chem. Res.*, 50 (2017) 1423-1432.

[15] G. Chen, S. Huang, X. Kou, F. Zhu, G. Ouyang, Embedding Functional Biomacromolecules within Peptide-Directed Metal-Organic Framework (MOF) Nanoarchitectures Enables Activity Enhancement, *Angew. Chem. Int. Ed. Engl.*, 59 (2020) 13947-13954.

[16] J. Liang, K. Liang, Biocatalytic Metal-Organic Frameworks: Prospects Beyond Bioprotective Porous Matrices, *Adv. Funct. Mater.*, 30 (2020) 2001648

[17] L. Chen, Q. Xu, Metal-Organic Framework Composites for Catalysis, *Matter*, 1 (2019) 57-89.

[18] Y. Chen, S. Han, X. Li, Z. Zhang, S. Ma, Why does enzyme not leach from metal-organic frameworks (MOFs)? Unveiling the interactions between an enzyme molecule and a MOF, *Inorg. Chem.*, 53 (2014) 10006-10008.

[19] S.S. Nadar, L. Vaidya, V.K. Rathod, Enzyme embedded metal organic framework (enzyme-MOF): De novo approaches for immobilization, *Int. J. Biol. Macromol.*, 149 (2020) 861-876.

[20] V. Lykourinou, Y. Chen, X.S. Wang, L. Meng, T. Hoang, L.J. Ming, R.L. Musselman, S. Ma, Immobilization of MP-11 into a mesoporous metal-organic framework, MP-11@mesoMOF: A new platform for enzymatic catalysis, *J. Am. Chem. Soc.*, 133 (2011) 10382-10385.

[21] T.J. Pisklak, M. Macías, D.H. Coutinho, R.S. Huang, K.J. Balkus, Hybrid materials for immobilization of MP-11 catalyst, *Top. Catal.*, 38 (2006) 269-278.

[22] S. Jung, S. Park, Dual-surface functionalization of metal-organic frameworks for enhancing the catalytic activity of candida antarctica Lipase B in polar organic media, *ACS Catal.*, 7 (2017) 438-442.

[23] P. Adlercreutz, Immobilisation and application of lipases in organic media, *Chem. Soc. Rev.*, 42 (2013) 6406-6436.

[24] Ruth Röder, Tobias Preiß, Patrick Hirschle, Benjamin Steinborn, Andreas Zimpel, Miriam Hoehn, Joachim O. Rädler, Thomas Bein, Ernst Wagner, Stefan Wuttke, U. Lächelt, Multifunctional nanoparticles by coordinative self-assembly of his-tagged units with metal-organic frameworks, *J. Am. Chem. Soc.*, 139 (2017) 2359-2368.

[25] J. Sun, Y. Fu, R. Li, W. Feng, Multifunctional hollow-shell microspheres derived from cross-Linking of MnO_2-nanoneedles by zirconium-based coordination polymer: enzyme mimicking, micromotors, and protein immobilization, *Chem. Mater.*, 30 (2018) 1625-1634.

[26] E.J. Baran, Metal complexes of carnosine, *Biochemistry*, 65 (2000) 789-797.

[27] A. Torreggiani, G. Fini, G. Bottura, Effect of transition metal binding on the tautomeric equilibrium of the carnosine imidazolic ring, *J. Mol. Struct.*, 565-566 (2001) 341-346.

[28] A.P. Katsoulidis, K.S. Park, D. Antypov, C. Marti-Gastaldo, G.J. Miller, J.E. Warren, C.M. Robertson, F. Blanc, G.R. Darling, N.G. Berry, J.A. Purton, D.J. Adams, M.J. Rosseinsky, Guest-adaptable and water-stable peptide-based porous materials by imidazolate side chain control, *Angew. Chem. Int. Ed. Engl.*, 53 (2014) 193-198.

[29] S. Kamari Kaverlavani, S.E. Moosavifard, A. Bakouei, Self-templated synthesis of uniform nanoporous CuCo2O4 double-shelled hollow microspheres for high-performance asymmetric supercapacitors, *Chem. Commun. (Camb.)*, 53 (2017) 1052-1055.

[30] L. Zhou, J. Li, J. Gao, H. Liu, S. Xue, L. Ma, G. Cao, Z. Huang, Y. Jiang, Facile oriented immobilization and purification of his-tagged organophosphohydrolase on viruslike mesoporous silica nanoparticles for organophosphate bioremediation, *ACS Sustain. Chem. Eng.*, 6 (2018) 13588-13598.

[31] G. Cao, J. Gao, L. Zhou, Z. Huang, Y. He, M. Zhu, Y. Jiang, Fabrication of Ni^{2+}-nitrilotriacetic acid functionalized magnetic mesoporous silica nanoflowers for one pot purification and immobilization of His-tagged ω-transaminase, *Biochem. Eng. J.*, 128 (2017) 116-125.

[32] G. Cao, J. Gao, L. Zhou, Y. He, J. Li, Y. Jiang, Enrichment and coimmobilization of cofactors and His-tagged ω-transaminase into nanoflowers: A facile approach to constructing self-sufficient biocatalysts, *ACS Applied Nano Materials*, 1 (2018) 3417-3425.

[33] P. Yang, L.J. Yang, Q. Gao, Q. Luo, X.C. Zhao, X.M. Mai, Q.L. Fu, M.Y. Dong, J.C. Wang, Y.W. Hao, R.Z. Yang, X.C. Lai, S.D. Wu, Q. Shao, T. Ding, J. Lin, Z.H. Guo, Anchoring carbon

nanotubes and post-hydroxylation treatment enhanced Ni nanofiber catalysts towards efficient hydrous hydrazine decomposition for effective hydrogen generation, *Chem. Commun.*, 55 (2019) 9011-9014.

[34] L. Feng, S. Yuan, L.L. Zhang, K. Tan, J.-L. Li, A. Kirchon, L.-M. Liu, P. Zhang, Y. Han, Y.J. Chabal, Creating hierarchical pores by controlled linker thermolysis in multivariate metal-organic frameworks, *J. Am. Chem. Soc.*, 140 (2018) 2363-2372.

[35] P.Q. Trombley, M.S. Horning, L.J. Blakemore, Interactions between carnosine and zinc and copper: implications for neuromodulation and neuroprotection, *Biochemistry (Mosc)*, 65 (2000) 807-816.

[36] H.C. Freeman, J.T. Szymanski, Crystallographic studies of metal-peptide complexes. V. (β-Alanyl-l-histidinato)copper(II) dihydrate, *Acta Crystallogr.*, 22 (1967) 406-417.

[37] J.L. A. Kirchon, F. Xia, G.S. Day, B. Becker, W. Chen, H.J. Sue, Y. Fang, H.C. Zhou, Modulation versus templating: fine-tuning of hierarchally porous PCN-250 using fatty acids to engineer guest adsorption, *Angew. Chem.*, 58 (2019) 12425-12430.

[38] S. Storck, H. Bretinger, W.F. Maier, Characterization of micro- and mesoporous solids by physisorption methods and pore-size analysis, *Appl. Catal. A-Gen.*, 174 (1998) 137-146.

[39] F. Zhang, M. Chen, X. Wu, W. Wang, H. Li, Highly active, durable and recyclable ordered mesoporous magnetic organometallic catalysts for promoting organic reactions in water, *J. Mater. Chem. A*, 2 (2014) 484-491.

[40] L. Jeong Woo, A. Taebin, S. Devaraj, K. Jang Myoun, K. Jong-Duk, Non-aqueous approach to the preparation of reduced graphene oxide/α-$Ni(OH)_2$ hybrid composites and their high capacitance behavior, *Chem. Commun.*, 47 (2011) 6305-6307.

[41] X. Luo, M. Huang, D. He, M. Wang, Y. Zhang, P. Jiang, Porous NiCo2O4 nanoarray-integrated binder-free 3D open electrode offers a highly efficient sensing platform for enzyme-free glucose detection, *Analyst*, 143 (2018) 2546-2554.

[42] J. Zhang, J. Zhang, Z. Jin, Z. Wu, Z. Zhang, Electrochemical lithium storage capacity of nickel mono-oxide loaded anatase titanium dioxide nanotubes, *Ionics*, 18 (2012) 861-866.

[43] G. Schenk, I. Mateen, T.K. Ng, M.M. Pedroso, N. Mitić, M.J. Jr, R.F.C. Marques, L.R. Gahan, D.L. Ollis, Organophosphate-degrading metallohydrolases: Structure and function of potent catalysts for applications in bioremediation, *Coord. Chem. Rev.*, 317 (2016) 122-131.

[44] F. Ely, K.S. Hadler, N. Mitić, L.R. Gahan, D.L. Ollis, N.M. Plugis, M.T. Russo, J.A. Larrabee, G. Schenk, Electronic and geometric structures of the organophosphate-degrading enzyme from Agrobacterium radiobacter (OpdA), *J. Biol. Inorg. Chem.*, 16 (2011) 777-787.

[45] J. Yang, K. Ni, D. Wei, Y. Ren, One-step purification and immobilization of his-tagged protein via Ni^{2+}-functionalized Fe_3O_4@polydopamine magnetic nanoparticles, *Biotechnol. Bioproc. E.*, 20 (2015) 901-907.

[46] H. Irene, T.D. Sutherland, R.L. Harcourt, R.J. Russell, J.G. Oakeshott, Identification of an opd (organophosphate degradation) gene in an Agrobacterium isolate, *Appl. Environ. Microbiol.*, 68 (2002) 3371-3376.

[47] Y. Jiang, L. Ma, L. Zhou, L. Ma, Y. He, X. Zhang, J. Gao, Structured interlocked-microcapsules: A novel scaffold for enzyme immobilization, *Catal. Commun.*, 88 (2017) 35-38.

[48] M.A. Prieto, J.A. Vazquez, M.A. Murado, A new and general model to describe, characterize, quantify and classify the interactive effects of temperature and pH on the activity of enzymes, *Analyst*, 140 (2015) 3587-3602.

[49] M. Taheran, M. Naghdi, S.K. Brar, E.J. Knystautas, M. Verma, R.Y. Surampalli, Degradation of chlortetracycline using immobilized laccase on polyacrylonitrile-biochar composite nanofibrous membrane, *Sci. Total Environ.*, 315 (2017) 605-606.

[50] M. Sarı, S. Akgöl, M. Karataş, A. Denizli, Reversible immobilization of catalase by metal chelate affinity interaction on magnetic beads, *Ind. Eng. Chem. Res.*, 45 (2006) 3036-3043.

[51] B. Koohshekan, A. Divsalar, M. Saiedifar, A.A. Saboury, B. Ghalandari, A. Gholamian, A.

Seyedarabi, Protective effects of aspirin on the function of bovine liver catalase: A spectroscopy and molecular docking study, *J. Mol. Liq.*, 218 (2016) 8-15.

[52] L. Wang, L. Wei, Y. Chen, R. Jiang, Specific and reversible immobilization of NADH oxidase on functionalized carbon nanotubes, *J. Biotechnol.*, 150 (2010) 57-63.

[53] S. Xue, J. Li, L. Zhou, J. Gao, G. Liu, L. Ma, Y. He, Y. Jiang, Simple Purification and Immobilization of His-Tagged Organophosphohydrolase from Cell Culture Supernatant by Metal Organic Frameworks for Degradation of Organophosphorus Pesticides, *J. Agric. Food Chem.*, 67 (2019) 13518-13525.

Declaration of interests

☒ The authors declare that they have no known competing financial interests or personal relationships that could have appeared to influence the work reported in this paper.

☐The authors declare the following financial interests/personal relationships which may be considered as potential competing interests: